Phys Chem Minerals (2004) 31: 240–246
DOI 10.1007/s00269-004-0390-2

ORIGINAL PAPER

H. Liu · J. Hu · J. Xu · Z. Liu · J. Shu · H. K. Mao
J. Chen

Phase transition and compression behavior of gibbsite under high-pressure

Received: 29 March 2003 / Accepted: 26 January 2004

Abstract In situ high-pressure synchrotron X-ray diffraction and infrared absorption experiments for gibbsite were performed at room temperature up to 53 and 25 GPa, respectively. A phase transition was confirmed at about 2.5 GPa. The high-pressure phase is indexed as an orthorhombic structure, rather than a triclinic structure as reported in previous studies. The compressibility of gibbsite and its high-pressure polymorph were studied, and their bulk moduli K_0 were determined to be 49 and 75 GPa, respectively with K_0' as 4. The in situ high-pressure infrared absorption spectra revealed the gradual disordering of hydrogen substructure above 15 GPa in quasihydrostatic compression.

Keywords $Al(OH)_3$ · High-pressure · Phase transition · X-ray diffraction · Infrared absorption

Introduction

The water reservoir in the Earth's mantle is one of the key subjects in geosciences, and recently Murakami et al. (2002) suggested that the Earth's lower mantle may store more water than the oceans after studying lower-mantle minerals synthesized in a natural peridotitic composition. Thus, knowledge of the high-pressure behavior of hydrous minerals is important to an understanding of the source of water, and its role in deep focus earthquakes in the Earth's mantle. In the aluminum trihydroxide case, four polymorphs, i.e., gibbsite [α-$Al(OH)_3$], bayerite [β-$Al(OH)_3$], nordstrandite [γ-$Al(OH)_3$], and doyleite, have been found in nature. Among them, gibbsite is one of the most abundant natural minerals in the aluminum hydroxide and oxide family, and has attracted experimental and theoretical attention from the point of view of mineralogical and industrial applications (e.g., Gale et al. 2001; Ruan et al. 2001; Digne et al. 2002; Johnston et al. 2002). In 1996, Huang et al. reported a high-pressure phase transition in gibbsite above 3 GPa from Raman spectra and X-ray diffraction, and the nordstrandite (triclinic structure) was proposed as a candidate for the quenchable high-pressure phase. In 1999, Huang et al. identified the high-pressure phase as nordstrandite from the improved data up to 10 GPa using high-pressure in situ angle-dispersive X-ray diffraction. Some hydrous minerals were found to become unstable upon further compression, such as amorphization in $Ca(OH)_2$ (Kruger et al. 1989; Nagai et al. 2000), or gradual disordering of the hydrogen sublattice in $Co(OH)_2$ (Nguyen et al. 1997; Parise et al. 1999; Shieh and Duffy 2002). Therefore, higher-pressure research on gibbsite to check its stability upon further compression was our original motivation. In this report, we carried out an in situ high-pressure study on gibbsite up to 53 GPa for XRD and 25 GPa for IR, respectively, at room temperature, and re-indexed the high-pressure phase as an orthorhombic structure. The high-pressure phase remained stable up to the maximum pressure reached in the XRD experiments, could be quenched when the pressure was released, and remained stable under ambient conditions for over 6 months. The gradual disordering behavior for the hydrogen sublattice above 15 GPa was observed from in situ high-pressure IR measurements during a quasihydrostatic compression process.

H. Liu (✉)
HPCAT, Advanced Photon Source,
Argonne National Laboratory, IL 60439–4803
e-mail: hliu@hpcat.aps.anl.gov
Tel.: +630 252 4058
Fax: +631-252-0496

J. Hu · J. Xu · Z. Liu · J. Shu · H. K. Mao
Geophysical Laboratory,
Carnegie Institution of Washington,
Washington DC 20015

J. Chen
Mineral Physics Institute,
State University of New York at Stony Brook,
NY, 11794-2100

Experimental

The energy-dispersive X-ray diffraction (EDXRD) experiments were carried out at beamline X17C (Hu et al. 2000) of National Synchrotron Light Source (NSLS), Brookhaven National Lab. T301 stainless steel gaskets with a hole diameter of about 100 microns for the sample chamber were used in a diamond-anvil cell (DAC). The gibbsite powder sample and several ruby chips were loaded in the DAC, with different pressure-transmitting media including helium, argon, and a methanol–ethanol (4:1) mixture, in different runs. A Ge solid-state detector was set at a two-theta angle of 10° to collect diffraction patterns. A small amount of sample with respect to the amount of pressure medium was loaded in the DAC to avoid the sample touching both diamond anvils during compression, and therefore to achieve a pressure which was more hydrostatic. This, together with the weakness of the X-ray scattering, resulted in a long acquisition time of a few hours to collect a high-quality diffraction pattern. The synthetic gibbsite powders from three sources (Alfa Aesar company, Baker company, offered by Huang et al. 1999, as well as the synthetic sample from Institute of Chemistry, Chinese Academy of Science, Beijing), were used as starting materials in the in situ high-pressure X-ray diffraction studies to check their phase-transition pressure. No obvious differences were observed within the experimental uncertainty.

The in situ high-pressure infrared absorption spectra of the sample over 600 to 4000 cm^{-1} range were collected on a Bruker IFS 66 s/V FTIR spectrometer with an MCT detector at beamline U2 A (Hemley et al. 2000) of NSLS. To avoid any saturated absorption, a thin sample pellet with thickness less than 5 μm and about 70 μm in diameter was pre-pressed, and then loaded in a T301 steel gasket hole, which was about 180 μm in diameter and about 40 μm in thickness, in an optical diamond (type-IIa) anvil cell. The high-pressure IR spectra were measured up to 25 GPa at room temperature. Argon was used as pressure medium. The ruby fluorescence method was used for pressure calibration in both XRD and IR experiments.

Results and discussions

Compressibility of gibbsite

X-ray diffraction patterns of $Al(OH)_3$ during compression up to 53 GPa in a methanol–ethanol pressure medium are shown in Fig. 1. The diffraction data of gibbsite were also collected in a helium pressure medium. Then the derived lattice parameters of gibbsite as a function of pressure are summarized in Table 1. The initial axis compressibility (see Fig. 2a) was found as $c/c_0 > a/a_0 > b/b_0$, while the β angle of monoclinic structure increases with pressure before the phase transition occurred. This behavior is in agreement with previous studies (Huang et al. 1999). Gibbsite is a layered-type compound, in which the layer consists of a stacking of AlO_6 octahedra with one shared edge along the *a*–*b* plane. Each oxygen atom links to one hydrogen atom,

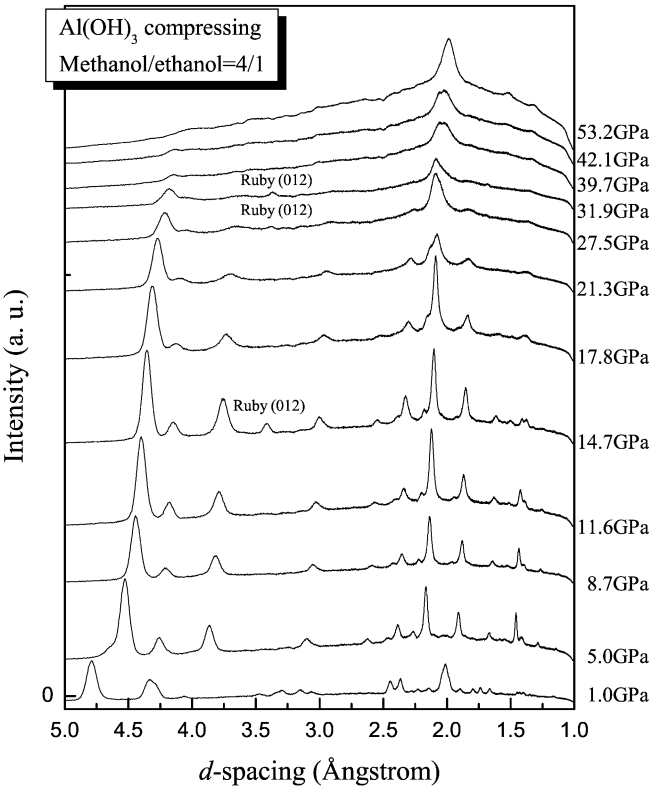

Fig. 1 Typical diffraction patterns of $Al(OH)_3$ upon compression to 53 GPa with methanol–ethanol mixture as pressure medium

Table 1 The compression data for gibbsite and its high-pressure polymorph. Most of the data listed in this table were derived from XRD data using methanol–ethanol as the pressure medium, while the data from helium as pressure medium are marked by * and were also used in the gibbsite's bulk modulus fitting. The uncertainties in pressure scale, cell parameters, β, and unit-cell volume are about ± 1%, ± 0.002 Å, ± 0.2°, and ± 0.3 $Å^3$, respectively

Gibbsite (monoclinic)						High-pressure phase (orthorhombic)				
P(Gpa)	*a* (Å)	*b* (Å)	*c* (Å)	*β* (°)	*V* ($Å^3$)	*P*(GPa)	*a* (Å)	*b* (Å)	*c* (Å)	*V* ($Å^3$)
0	8.655	5.073	9.716	94.6	425.2	5.0	8.529	4.968	9.050	383.4
0.7*	8.603	5.051	9.628	94.8	416.9	8.7	8.412	4.900	8.895	366.6
1.0	8.611	5.046	9.618	94.8	416.4	11.6	8.360	4.859	8.799	357.4
1.2*	8.552	5.041	9.618	95.2	412.9	14.7	8.295	4.829	8.703	348.6
3.2*	8.550	4.991	9.482	96.0	402.4	17.8	8.254	4.791	8.622	340.9
5.0	8.534	4.970	9.269	96.2	390.8	21.3	8.188	4.750	8.545	332.3
						23.5	8.132	4.730	8.499	326.9
						25.3	8.109	4.720	8.480	324.5
						27.5	8.089	4.701	8.434	320.7
						29.4	8.069	4.699	8.405	318.6
						31.9	8.050	4.659	8.371	313.9

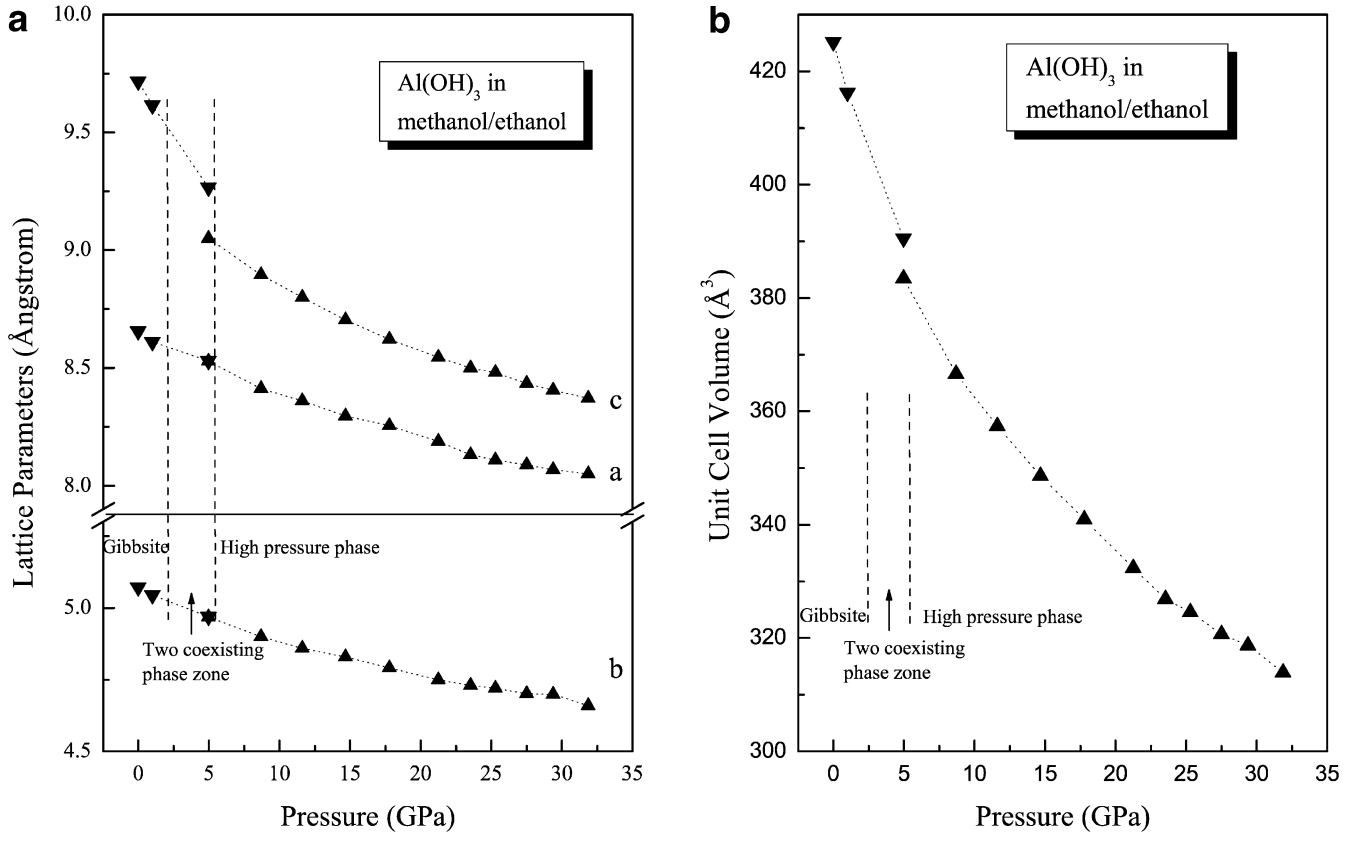

Fig. 2a The pressure dependence of lattice parameters *a*, *b*, *c* of gibbsite and its high-pressure phase (methanol–ethanol mixture as pressure medium; the error bars are omitted since they are smaller than the symbol size). **b** The unit-cell volume change of gibbsite and its high-pressure phase under pressure (methanol–ethanol mixture as pressure medium; the error bars are omitted since they are smaller than the symbol size)

while half of the hydrogen atoms form the intralayer hydrogen bond in the *a*–*b* plane and the other half form the interlayer hydrogen bonds along the *c* direction. The structural features of gibbsite, i.e., weaker bond direction along layers, make its *c* axis more compressible at the beginning of compression. This is a common behavior in hydrous minerals with layered-type structure.

The bulk modulus of gibbsite was experimentally reported as 85 GPa by Huang et al. in 1999. However, it is in contrast with the simulation result by ab initio quantum-mechanical calculations reported by Gale et al. in 2001, in which the bulk modulus of gibbsite was estimated as 55 GPa. The unreasonably large difference (about 35%) between the experimental and theoretical simulation results was explained as possible impurities in experimental sample, such as sodium cations; these made the bond between layers stronger than the hydrogen bond alone, thus raising the bulk modulus. Therefore further calculations are being done to determine the influence of sodium doping on the gibbsite (Gale et al. 2001).

In this study, we also derived the bulk modulus by fitting volume vs. pressure data of gibbsite to the second-order Birch equation of state (EoS). In total, six experimental data (in Table 1), including the data from two coexisting phases, were used in the fitting. Figure 3 illustrates the experimental data and the fitting result, while the data from Huang et al. (1999) were also plotted for comparison. There is some pressure offset between the two sets of experimental data. Huang et al. used Au as a pressure calibration material while we used ruby fluorescence. The difference between these two pressure calibrations is always very small at a

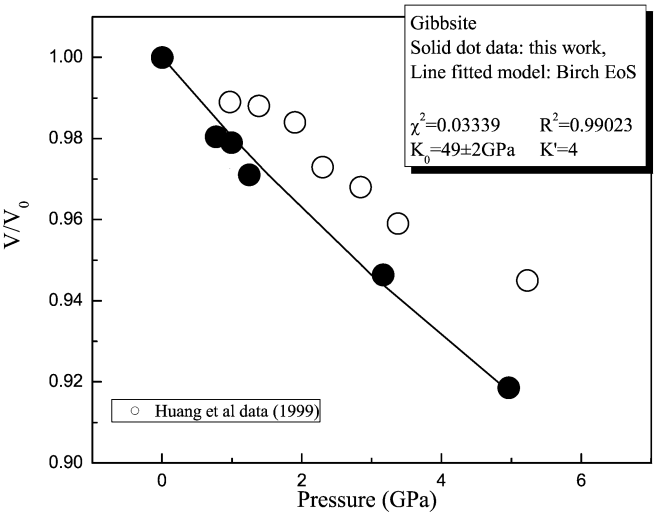

Fig. 3 The EoS fitting results of the gibbsite, the error bars are omitted since they are smaller than the symbol size

Table 2 Pressure dependence and mode Grüneisen parameters of IR frequencies of OH bands in $Al(OH)_3$

	Gibbsite			High-pressure phase (below 15 GPa)		High-pressure phase (above 15 GPa)	
	ν_0 (cm^{-1})	$d\nu/dp$ (cm^{-1} GPa^{-1})	γ_G	$d\nu/dp$ (cm^{-1} GPa^{-1})	γ_G	$d\nu/dp$ (cm^{-1} GPa^{-1})	γ_G
ν $(OH)_1$	3619	−0.9	−0.012				
ν $(OH)_{2*}$	3586	−16.9	−0.231	−11.9			
ν $(OH)_4$	3528	−10.3	−0.178				
ν $(OH)_h$				−12.0	−0.257	−8.0	−0.174
ν $(OH)_6$	3485	−18.5	−0.260	−14.3			
ν $(OH)_3$	3395	−24.9	−0.359				
ν $(OH)_5$	3375	−32.3	−0.469				
δ (OH)	913	3.6	0.192				
δ (OH)	979	9.9	0.490	4.9	0.366	3.5	0.258
δ (OH)	1023	6.3	0.299				

low-pressure range within 5 GPa. One possible reason for the offset may be partly attributed to the different unit-cell volume under ambient conditions used. The smaller unit-cell volume of 418.1 $Å^3$ (Table 2 in Huang et al. 1999) than that in JCPDS card as 425.168 $Å^3$ under ambient conditions could produce a higher bulk modulus value. In this report, the measured unit-cell parameters ($a = 8.655$ Å, $b = 5.073$ Å, $c = 9.716$ Å, $\beta = 94.6^0$ and $V_0 = 425.2$ $Å^3$) from the refinement of the XRD pattern under ambient conditions are very close to the values in the JCPDS card (No. 33-0018) for gibbsite. Then the bulk modulus K_0 is estimated as 49 ± 2 GPa by setting its pressure derivative K_0' as 4.

This K_0 value is between the simulation results of 55 and 45 GPa, the latter derived directly from interatomic potentials (Gale et al. 2001). This means that the density functional approach base calculation did not really fail in the bulk modulus issue of gibbsite; instead, if compared with the experimental K_0 value in this report, it worked very well as in previous cases of a variety of compounds. It is probably understandable that Gale et al.'s simulation slightly overestimated the bulk modulus value as 55 GPa. In their simulation, the gibbsite structure was optimized and the volume was overestimated by about 4% from experimental data. The most significant discrepancy was from the β angle of monoclinic gibbsite, which was estimated to be smaller than experimental data. This may enhance the bond between layers and thus give a bigger bulk modulus. The improvement of the theoretical optimized structure of gibbsite, which was close to experimental values by using extensive optimization of basis functions, was reported by Digne et al. (2002) in a similar calculation method. The elastic constants of gibbsite based on the theoretical simulation (Digne et al. 2002) will be very helpful in further high-pressure single-crystal experimental research.

Crystal structure of the high-pressure phase and its compressibility

A phase transition around 3 GPa was observed by Huang et al. in 1996 and 1999, and the high-pressure phase was identified as nordstrandite structure with triclinic symmetry. In this report, various pressure media were used to confirm the phase-transition pressure, and no obvious pressure medium dependence was observed. The new phase diffraction peaks appeared around 2.5 GPa, and the phase transition was completed as pressure reached 5 GPa. In fact, Dachille and Gigl first reported a high-pressure phase from gibbsite in 1983 using an opposed-anvils apparatus, and the high-pressure phase appeared above 1.5 GPa even at room temperature. A slow conversion rate from gibbsite resulted in the concentration of the high-pressure phase as 30–60% in the final sample mixture. In spite of the difficulty of the phase identification from the two coexisting phase samples, they already ruled out the possibility of the high-pressure phase as any known $Al(OH)_3$ polymorph by comparison of the XRD and IR spectra. Then the unknown high-pressure phase was indexed as a monoclinic structure with β angle as 90.48^0 (Dachille and Gigl 1983). The assignment for the irreversible high-pressure phase as nordstrandite was not reasonable from the high-resolution angle-dispersive XRD data (Huang et al. 1999). For example, the most important new strong peak in the quenched new phase with $d = 3.978$ Å (image plate data, Table 1 in Huang et al. 1999), was assigned as $d = 4.160$ Å and $d = 3.896$ Å of nordstrandite; this is obviously out of the experimental uncertainty range of the angle-dispersive XRD. In the previous reports (Huang et al. 1996, 1999), the *hkl* index of the nordstrandite phase was also completely different from the JCPDS card in spite of the claim of it's being cited from the JCPDS card.

In this report, the simpler XRD patterns after the pressure-induced phase transition encouraged us to re-index this high-pressure phase as orthorhombic. It was difficult to correctly index the two phases in the coexisting range around 2.5–5.0 GPa. Indexing became clear in the pure high-pressure phase at higher pressure. Figure 4 shows a typical LeBail refinements result for the XRD pattern of the high-pressure phase under 8.7 GPa by using the GSAS package (Larson and Von Dreele 1994), and clearly indicates the high-pressure phase as an orthorhombic structure. The orthorhombic structure is most likely a transformation by the layer's shifting its β angle to

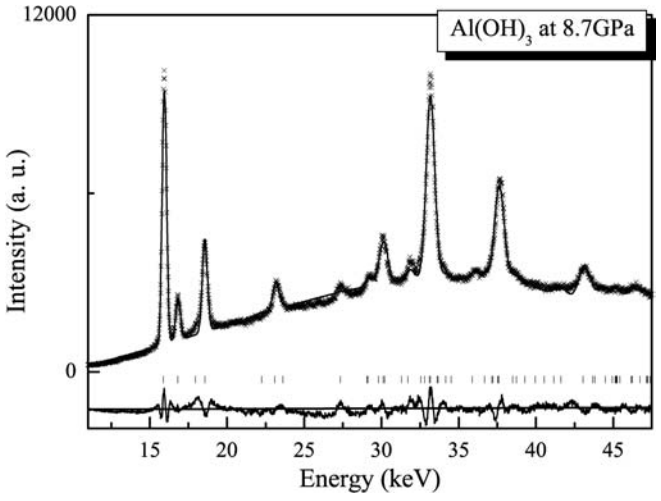

Fig. 4 The LeBail refinement result for XRD pattern of the $Al(OH)_3$ high-pressure polymorph at 8.7 GPa, in which $R_{wp} = 5.69\%$, $R_p = 4.10\%$

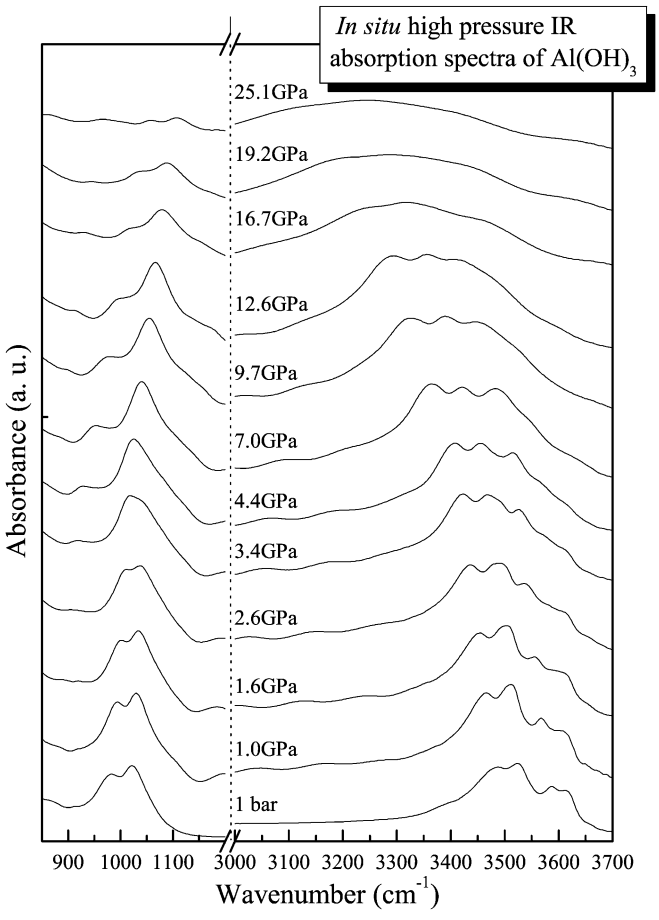

Fig. 5 In situ high-pressure IR absorption spectra up to 25 GPa at room temperature

90° while keeping other structural features similar to those of gibbsite. The high-resolution angle-dispersive diffraction data are required to refine the high-pressure phase, at least to obtain the structural information for the Al–O framework change, and the corresponding high-pressure work is in progress. The lattice parameters of the high-pressure phase were listed in Table 1 and plotted in Fig. 2a, in which the data were available up to 31.9 GPa since the broader diffraction peaks at higher pressure resulted in a great uncertainty in the refined parameters. The second-order Birch EoS fitting for the high-pressure phase was also performed by using the data in Table 1, and its bulk modulus was 75 ± 2 GPa while $K_0' = 4$. Under ambient conditions, the quenched new phase was refined ($a = 8.690$ Å, $b = 5.044$ Å, $c = 9.500$ Å) and its unit-cell volume was 416.4 $Å^3$, which was about 2% smaller than the unit-cell volume of gibbsite under ambient conditions, while the molar volume of the nordstrandite phase is larger than gibbsite.

The XRD method provides limited information for light elements, and is nearly blind to hydrogen. The accurate structural information for the role of hydrogen could be achieved from the spectroscopic studies such as Raman and IR, which are more sensitive to the change relative to hydrogen bonds. Frost et al. reported a systemic study of the vibrational spectroscopy of gibbsite from various synthetic and natural sources in 1999. In 2000, Wang and Johnston made an assignment of OH-stretching modes of gibbsite, in which the interlayer and intralayer OH vibrations were resolved by using polarized single-crystal Raman spectroscopy. All these works helped us to obtain more information from the high-pressure IR spectra. The in situ high-pressure IR spectra up to 25 GPa at room temperature are shown in Fig. 5. Figure 6 demonstrates the corresponding pressure dependence of the mode shifts of OH vibrational and deformation bonds in $Al(OH)_3$, in which the stretching bands from the intralayer group OH_1 at 3619 cm^{-1}, interlayer groups OH_3 and OH_5 at 3395 and 3375 cm^{-1} began to disappear during the phase-transition process. These indicate that the original six unique OH groups with the hydrogen and oxygen occupying the low site symmetry in the gibbsite crystal structure decreased their IR active mode number, and support our XRD result in which the high-pressure phase was indexed as higher symmetrical structure. The intralayer OH_2 group was reported between the OH_1 and OH_4 group (Wang and Johnston 2000), thus we attributed the 3585 cm^{-1} mode under ambient conditions and the corresponding mode in high-pressure IR spectra also to intralayer groups and marked as OH_{2*} vibrational mode. The cause of the difference between their frequencies under ambient conditions is still unclear.

Before the phase transition occurred, all ν(OH) modes in the gibbsite phase shifted to lower frequencies due to compression enhanced the hydrogen-bonding strength. The three interlayer ν(OH) modes at lower frequencies shifted more than the three at higher frequencies for intralayer modes. This difference could be understood as greater compression along the layer direction (c axis) with pressure, and this was similar to the low-temperature-induced ν(OH) bands' red shift trend which was caused by thermal lattice compression. Wang and

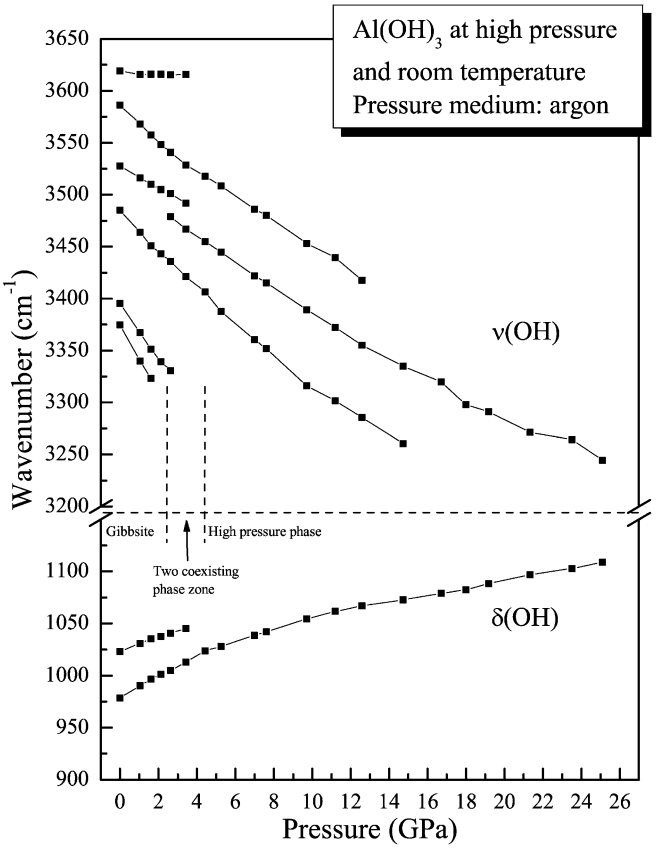

Fig. 6 The pressure dependence of the mode shifts of OH-stretching and deformation modes in $Al(OH)_3$

Johnston pointed out that because of the intrinsically weak coupling of the ν(OH) vibration with the crystal structure, the positions of the intra- and interlayer modes with different crystalline symmetry are expected to be similar, if not to degenerate. Thus we assume that the continuing parts of ν(OH) corresponding to intralayer OH_{2*} and interlayer OH_6 still indicate that their OH group is located at intralayer and interlayer positions, respectively, in the high-pressure phase, while it is unclear whether the peak located between them marked as $\nu(OH)_h$ is from intra- or interlayer modes.

Disordering of hydrogen sublattice in the high-pressure phase

Argon was used as pressure medium in the IR measurement, which generates a quasihydrostatic pressure condition to minimize the effect of stress-induced IR band broadening. The ν(OH) peaks became further broadened above 15 GPa and the vibrational modes merged together. Further compression resulted in a more broadened band with a peak width around 300–400 cm^{-1} within the experimental pressure range up to 25 GPa. These indicated a broad distribution of OH bond length, angle, and strength in the sample, and it was attributed to the gradual disordering of the hydrogen sublattice upon compression in the pressure interval of 15–25 GPa. Table 2 lists the pressure dependence of these OH modes in the sample, and their mode Grüneisen parameters, $\gamma_{iG} = -\frac{d\ln v_i}{d\ln V} = \frac{K_0}{v_{i0}}\left(\frac{dv_i}{dP}\right)$, also were calculated by using the slope dv_i/dP of each mode, and the bulk modulus for the gibbsite and its high-pressure phase obtained from XRD in this report. The slopes of dv_i/dP of IR-active modes, which were fitted assuming linearly dependence with pressure, changed abruptly around the phase transition, and two obvious regions were separated around 15 GPa in the high-pressure phase. The OH-stretching bands were taken as describing the time-averaged hydrogen bond-strength distribution throughout the sample, with a continuous range of bond strengths caused by the positional disorder of the hydrogen atoms and their possible varying involvement in intra- and interlayer hydrogen bonds under compression above 15 GPa.

The corresponding high-pressure Raman spectra were measured by Huang et al. (1996) up to 23 GPa, and three additional peaks in OH-stretching modes' range appeared above 3 GPa. More OH vibrational modes were derived from the broadened Raman signals from the high-pressure phase. However, very recently, Johnston et al. (2002) reported a single-crystal high-pressure Raman spectra for gibbsite up to 5.5 GPa. The phase transition occurred around 2.2 GPa while only three Raman-active modes for the OH-stretching vibrational band were observed for the pure high-pressure phase. The latter results were in agreement with our high-pressure IR results for the less active modes of OH vibrations, and also supported the XRD result for a higher symmetry (orthorhombic) structure than gibbsite. If we take a closer look at the gibbsite powder Raman spectra reported earlier (Fig. 3b in Huang et al. 1996), only the two coexisting phase ranges clearly had more peaks. The Raman bands became broadened at a higher-pressure range, thus the pressure dependence of the OH vibrational modes above the phase transition in Fig. 4b of Huang et al. (1996) was not very reasonable. From the high-pressure IR result discussed in this study, the further broadened Raman peaks above 11 GPa (Fig. 3b in Huang et al. 1996), could at least be partly explained by the beginning of the hydrogen substructure disordering.

$Co(OH)_2$ is one of the well-studied layered-type hydrous minerals under high-pressure. Nguyen et al. (1997) reported a partial amorphization under pressure from Raman and XRD data with the hydrogen sublattice amorphization abruptly occurring at about 11.2 GPa. Parise et al. (1999), from neutron-scattering data for $Co(OD)_2$, revealed a highly disordered but crystalline proton arrangement and the spectroscopic anomaly was attributed to a hydrogen repulsion transition. Very recently, Shieh and Duffy (2002) reported higher-pressure Raman and XRD results, and a gradual disordering of the hydrogen substructure over a broad pressure interval was observed. In spite of the fact that the $Al(OH)_3$ case is more complicated, since both interlayer and intralayer hydrogen bonds play

roles upon compression while $Co(OH)_2$ has only interlayer hydrogen bonds, to some extent a similarity between them still exists. Similarly to the $Co(OH)_2$ case, the high-pressure IR of $Al(OH)_3$ also indicated the gradual disordering of the hydrogen sublattice because of its broadened IR vibrational modes above 15 GPa, while the Al–O substructure still remained stable according to the corresponding XRD data. Just as Shieh and Duffy (2002) pointed out, the disordering of hydrogen may induce a small amount of local disordering in the Al–O basic structure, but is insufficient to drive the system to complete amorphization under compression. The further broadening of XRD patterns above 30 GPa demonstrated to some extent the disorder distribution of the Al–O substructure, but they still retained the "crystalline" instead of complete amorphization within the experimental range up to 53 GPa.

The important contribution of broadening of OH vibrational modes from the hydrogen bond angle distribution in hydrous minerals upon compression was highlighted by Hofmeister et al. in 1999. In this case, the hydrogen bond length was expected to become a little shorter while their bond angle decreases further with compression, especially for the interlayer hydrogen bond during the phase transition in which the lattice parameter of *c* along the layer abruptly decreased while the *a* and *b* decreased smoothly (Fig. 2a). Because of the lack of precise assignment and possible confusion by the overtone, the contributions of the lattice vibrations at lower frequencies are not discussed in this paper. The ab initio simulations are invited to reveal more information in the electronic structure level for the role of intra- and interlayer OH–O hydrogen bond changes, such as bond length and angle, during phase transition, as well as the detailed mechanism of the hydrogen substructure disordering process at higher pressure. This is possible to carry out in current, well-developed calculation methods, for example, by the Car–Parrinello molecular dynamics method.

The aluminum trihydroxides are chiefly crustal minerals in a silicate-poor region, but may play a role as water source in the mantle. The four polymorphs have been found naturally, and the newest one, doyleite, was first reported in 1985 (Chao et al. 1985; Clark et al. 1998). The quenchable high-pressure phase, which could completely transform from gibbsite above 5 GPa and remain stable under ambient conditions for at least 6 months from the sample in this study, is possibly found in nature if it is really stable in the mantle and crust environments. In fact, two of the known $Al(OH)_3$ phases (bayerite and nordstrandite) were synthesized in the laboratory before their discovery in nature.

Acknowledgements The authors thank Dr. E. Huang for the sample, as well as two reviewers for comments and help from Prof. J. A Tyburczy during the review process. H. L. thanks Dr. M. Vaughan and other former colleagues at Stony Brook for helpful discussions. This work was performed within COMPRES, which was supported by the National Science Foundation.

References

Chao GY, Baker J, Sabina AP, Roberts AC (1985) Doyleite, a new polymorph of $Al(OH)_3$, and its relationship to bayerite, gibbsite and nordstrandite. Can Mineral 23: 21–28

Clark GR, Rodgers KA, Henderson GS (1998) The crystal chemistry of doyleite, $Al(OH)_3$. Z Kristalogr 213: 96–100

Dachille F, Gigl P (1983) Two high-pressure $Al(OH)_3$ phases and contributions to the Al–Al_2O_3–H_2O system, High Temp High Press 15: 657–675

Digne M, Sautet P. Raybaud P, Toulhoat H, Artacho E (2002) Structure and stability of aluminum hydroxides: a theoretical study. J Phys Chem 106: 5155–5162

Frost RL, Kloprogge JT, Russell SC, Szetu JL (1999) Vibrational spectroscopy and dehydroxylation of aluminum (oxo)hydroxides: gibbsite. Appl Spectrosc 53: 423–434

Gale JD, Rohl AL, Milman V, Warren MC (2001) An ab initio study of the structure and properties of aluminum hydroxide: gibbsite and bayerite. J Phys Chem (B) 105: 10236–10242

Hemley RJ, Goncharov A, Liu ZX, Mao HK, Merkel S (2000) High-pressure infrared synchrotron and Raman microspectroscopy of Earth and planetary materials. In: Williams DB, Shimizu R (eds) Microbeam analysis 2000, pp 87–88

Hofmeister AM, Cynn H, Burnley PC, Meade C (1999) Vibrational spectra of dense, hydrous magnesium silicates at high-pressure: importance of the hydrogen bond angle. Am Mineral 84: 454–464

Hu JZ, Mao HK, Guo QZ, Hemley RJ (2000), High-pressure X-ray diffraction at X17C of the NSLS. In: Manghnani MH, Nellis WJ, Nicol MF (eds) Science and technology of high-pressure. Proceedings of AIRAPT-17 Honolulu, 25–30, July 1999, Universities Press, Hyderabad, India, pp 1039–1042

Huang E, Li A, Xu JA, Chen RJ, Yamanaka T (1996) High-pressure phase transition in $Al(OH)_3$: Raman and X-ray observations. Geophys Res Lett 23: 3083–3086

Huang E, Lin JF, Xu J, Huang T, Jean YC, Sheu HS (1999) Compression studies of gibbsite and its high-pressure polymorph. Phys Chem Miner 26: 576–583

Johnston CT, Wang SL, Bish DL, Dera P, Agnew SF, Kenney JW (2002) Novel pressure-induced phase transformations in hydrous layered materials. Geophys Res Lett 29: 171–174

Kruger MB, Williams Q, Jeanloz R (1989) Vibrational spectra of $Mg(OH)_2$ and $Ca(OH)_2$ under pressure. J Chem Phys 91: 5910–5915

Larson AC, Von Dreele RB (1994) General structure analysis system (GSAS), Los Alamos National Laboratory Report LAUR 86–748

Murakami M, Hirose K, Yurimoto H, Nakashima S, Takafuji N (2002) Water in Earth's lower mantle. Science 295: 1885–1887

Nagai T, Ito T, Hattori T, Yamanaka T (2000) Compression mechanism and amorphization of portlandite, $Ca(OH)_2$: structural refinement under pressure. Phys Chem Miner 27: 462–466

Nguyen JH, Kruger MB, Jeanloz R (1997) Evidence for "partial" amorphization in $Co(OH)_2$. Phys Rev Lett 78: 1936–1939

Parise JB, Loveday JS, Nelmes RJ, Kagi H (1999) Hydrogen repulsion "transition" in $Co(OD)_2$ at high-pressure? Phys Rev Lett 83: 328–331

Ruan HD, Frost RL, Kloprogge JT (2001) Comparison of Raman spectra in characterizing gibbsite, bayerite, diaspore and boehmite. J Raman Spectrosc 32: 745–750

Shieh SR, Duffy TS (2002) Raman spectroscopy of $Co(OH)_2$ at high-pressures: implications for amorphization and hydrogen repulsion. Phys Rev (B) 66: 134301–7

Wang SL, Johnston CT (2000) Assignment of the structural OH-stretching bands of gibbsite. Am Mineral 85: 739–744